ES Food and Agroforestry
DOI: https://dx.doi.org/10.30919/faf1932

Development of a Predictive Model of Water Hyacinth Drying in Solar Parabolic Dome with Artificial Neural Networks

J. Jongpluempiti,[1] P. Vengsungnle,[1] S. Poojeera,[2] A. Srichat,[3] A. Siricharoenpanich[4] and P. Naphon[4,*]

Abstract

Water hyacinth benefits humans and the environment. Cellulose makes water Hyacinth a biofuel. It encourages eco-friendly furniture, décor, and toys. This study dries hyacinths of various sizes in a solar parabolic dome to investigate how they dehumidify and then builds an artificial neural network model to forecast relative humidity. This study includes statistical and artificial neural network analysis at all experimental stages. Drying conditions in solar parabolic greenhouses reveal that all three hyacinth sizes dehumidify over time, decreasing the moisture ratio. These differences may be due to a tighter internal fiber structure or crust formation on the material's surface during baking, which slows water evaporation from the inside to the outside. This illustrates that material size affects dehumidification performance. Operating time and Hyacinth size affect the drying rate. We assessed the model's performance using R^2 and MSE values. These studies show that a few nodes may regulate automated and industrial drying processes. ANNs simplify machine learning and optimization by revealing complex data patterns and linkages, which are crucial for time series prediction, classification, and regression. Big data can help them improve over time.

Keywords: Water hyacinth; Artificial neural network; Biofuel; Environment.
Received: 24 October 2025; Revised: 25 November 2025; Accepted: 08 December 2025
Article type: Research article.

1. Introduction

The floating aquatic plant, water hyacinth, benefits humans and the environment. Since it absorbs toxins and nutrients, it improves wastewater quality. The high cellulose content of water hyacinth biomass makes it a potential biofuel ingredient. By offering a raw material for toys, furniture, and ornaments, it promotes eco-friendly crafting. Providing aquatic species habitats boosts biodiversity. Many pros and cons are evident.

Advantages

- Water Purification: Hyacinths in the water can improve water quality by removing excess nutrients and contaminants.
- Habitat Creation: It promotes biodiversity by providing a home for a variety of aquatic creatures.
- Soil Improvement: It improves soil fertility and structure when it breaks down.
- Economic Uses: Animal feed, biofuel, and craft materials can all benefit from it..

Disadvantages

- Invasive Species: The rapid spread of water hyacinths can clog streams and disrupt local ecosystems.
- Water Flow Blockage: It can impede water flow, leading to flooding and negatively affecting navigation.
- Impact on Fisheries: The decline in oxygen levels caused by its expansion could harm fish populations.

In solid-state fermentation, Mukherjee *et al*.[1] found that three white-rot fungi enhanced water hyacinth biomass dry matter digestibility. After 32 days, P. sajor-caju grew 20.4%. Organic components degraded fastest, losing 23.6% of their dry weight over 48 days. After 32 days of incubation with P. sajor-caju, the bioconverted biomass contained 1.1% soluble nitrogen on a dry-weight basis. Water hyacinth petiole drying rates (mean k) increased with oven drying temperature, according to Akendo *et al*.[2] K averaged 2.22 h-1 at 105 °C, 2.71 at 130 °C, and 3.39 at 150 °C. Results indicate that higher temperatures increase drying. At 16 analyses, water hyacinth petioles had 91% (wb) moisture. Samples from four Nairobi Dam sites have similar starting moisture content (P = 0.94). Hexavalent chromium (Cr(VI)) can be best removed from water hyacinth biomass at pH 2.0, 300 mg/L starting metal ion concentration, and 40 °C, according to Hasan *et al*.[3] Removal

[1]*Department of Agricultural Machinery Engineering, Faculty of Engineering and Architecture, Rajamangala University of Technology Isan, Nakhonratchasima, 30000, Thailand*
[2]*Department of Mechanical Engineering, Faculty of Engineering, Rajamangala University of Technology Isan, Khon Kaen, 40000, Thailand*

capacity was estimated at 91.5181 mg/g. As predicted by a Langmuir sorption isotherm model, water hyacinth biomass sorption capacity was 101 mg/g at 40 °C and pH 2.0. As Ighodalo *et al*.[4] showed, water hyacinth biomass briquettes are a good alternative to kerosene. Water hyacinth briquettes boiled water and cooked Indomie, rice, and yams practically as fast as kerosene stoves. Casas *et al*.[5] optimized the drying of water hyacinth. Drying temperature, airflow rate, and pass count affected reaction characteristics in the study. Research recommends drying water hyacinth at 90 °C, with an airflow rate of 0.044 m^3/s and five passes. These conditions dried best. DWH can absorb source-isolated human urine, according to Weng *et al*.[6] Absorption averaged 18.78 mL/g after 7 days, with 3.46% UDS recovered in urine. After rising from 0.46% to 3.14%, DWH phosphorus was recovered. The phosphorus-rich fertilizer made from DWH can be used as a foliar spray to enhance fruiting and flowering. The 60-day urine absorption system supports environmental sustainability and agriculture. The multi-tray solar drier dried water hyacinth (WH) 1.5-2 times faster than sun drying, and 50% faster than sun drying, according to Shoughy *et al*.[7] Dried compressed WH samples faster. For complete and compressed WH drying, the logarithmic drying model best explained and validated experimental data. The model with the highest coefficient of determination (0.997) and the lowest χ^2, MBE, and RMSE values was deemed the most effective.

Rezania *et al*.[8] highlighted water hyacinth's high combustible fuel value, material strength, and burning capacity when discussing its use as fuel briquettes. Jongmeesuk *et al*.[9] found that water hyacinth processed with 2.0% v/v sulfuric acid and 2.0% w/v sodium hydroxide, and autoclaved at 121 °C for 15 minutes, produced the highest levels of reducing sugars, 15.63 and 2.35 g/L. This enzyme was used to hydrolyze water hyacinth for the first time after 48 hours at 50 °C and a loading of 0.30 ml/g. The sugar level dropped to 11.95 g/L. Mukaratirwa *et al*.[10] discovered that untreated water hyacinth root biomass exhibited exothermic adsorption, with enthalpy values ranging from -51.234 kJ mol−1 for acetone to -74.658 kJ mol−1 for dichloromethane. Polar solvents included ethyl acetate, diethyl ether, dichloromethane, and acetone. Mineral acids and organic solvents are used to process water hyacinth root biomass. All solvents had a lower enthalpy of absorption due to lower acidity and Lewis basicity. The treatment decreases polar liquid absorption by biomass. Windarti *et al*.[11] studied the hydrolysis of dried water hyacinth (Eichhornia crassipes) biomass. A sulfuric acid catalyst yielded 0.38%, while a hydrochloric acid catalyst yielded 0.01%. Furfural was identified and characterized using the Fehling test, FTIR, ^{1}H NMR, and GC. According to Sukarni *et al*,[12] water hyacinth biomass thermally decomposes in four stages during pyrolysis. Stage II (active pyrolysis) occurs between 128 and 492 °C and releases 57% of the biomass mass as volatile chemicals. In the active pyrolysis zone, the Coats-Redfern method showed an activation energy of 60.74 kJ/mol, a logarithmic frequency factor of 4.77/min, and a reaction order of 1.9 for thermal degradation. Water hyacinth bio-boards, classed as high-density by Rahmawati *et al*.[13] meet the American National Standard for particle boards with a density range of 1.057 to 1.279 g/cm^3. Bio-boards' average bending rupture stress was 46.21 MPa, and tensile rupture stress was 6.64 MPa, proving their mechanical strength. With pressure, bio-board tensile strengths ranged from 5.73 MPa at 2 MPa to 7.61 MPa at 6.5 MPa. No significant relationship was observed between loading pressure and bending strength, with 2 MPa ideal for high-bending bio-boards. Yetti *et al*.[14] used Trichoderma viride cellulase enzymes to hydrolyze water hyacinth (Eichhornia crassipes) into microcrystalline cellulose. The final MCC was starch-free, organoleptic, water-soluble, drying shrinkage-free, and British Pharmacopoeia-listed. Functional groups, surface morphology, and thermal characteristics were analyzed using FTIR, SEM, and DSC. MCC melted at 93.196 °C, like Vivacel PH 102. Amante *et al*.[15] invented a machine that chops dry water hyacinth stalks into 0.5, 0.25, and 0.75 inches without human intervention. This method should help the local handicraft sector produce more high-quality pre-cut stalks. Worker emphasis may shift to weaving. Due to its high protein and amino acid profile, Rajan *et al*.[16] used water hyacinth as a sustainable feed for horses, pigs, and poultry to boost growth and productivity. It can enhance chicken egg output, reduce fish feed costs, and be used as cattle ensilage or as dried feed as a soybean meal substitute. Sustainable water hyacinth control boosts the economy. Water hyacinth is used to make paper, cardboard, disposable dinnerware, and other industrial products in addition to animal feed. Thang[17] observed that water hyacinth fibers treated with alkaline, soap, and water improved the mechanical properties of the green composite. Water hyacinth/roving composites improved after chemical treatment, as microstructural investigation revealed changes in fiber surface roughness and organization.

According to Nguyen *et al*.[18] water hyacinth fibers treated with alkaline solution, soap, and water improved the flexural and compressive strengths of green composites. Chemical treatment improved composite material properties by roughening the fiber surface and altering the arrangement of water hyacinth fibers, as shown by scanning electron microscopy (SEM). Bleached water hyacinth paper had densities of 21.68 g/m^3, average tensile rupture stresses of 1.337 MPa, Young's modulus of 36.278 MPa, and elongation at break of 4.744%, according to Wembe *et al*.[19] Comparatively, unbleached paper had a density of 26.37 g/m^3, a tensile strength of 0.405 MPa, and a compressive strength of

[3]*Department of Mechanical Engineering, Faculty of Technology and Engineering, Rajabhat University, Udon Thani, 41000, Thailand*
[4]*Department of Mechanical Engineering, Faculty of Engineering, Srinakharinwirot University, 63 Rangsit-Nakhornnayok Road, Ongkharak, Nakhorn Nayok, 26120, Thailand*
[*]*Email:* paisarnn@g.swu.ac.th (P. Naphon)

17.604 MPa. Unbleached paper is superior for packaging, seedling pots, mulching, and insulation, the study concluded, especially when water hyacinth is plentiful. In wet/dry cycles, natural rubber (NR) coatings improve the performance of water hyacinth (WH) geotextiles, according to Prongmanee *et al*.[20] Coated specimens are more durable because NR coatings limit fluctuations in water content and retain the fiber structure. The reduced water absorption, increased ultimate tensile strength (14.8 kN/m), and 20% matching strain at break make NR-coated WH geotextiles ideal for erosion control and installation with minimal damage from sharp, coarse stones. Rosidah *et al*.[21] found that ZnCl2-activated water hyacinth roots exhibited an optimal adsorption capacity (Qe) of 8.13 mg/g and an absorption efficiency (Ef) of 34.20% after 45 minutes. After 8 hours, roots carbonized at 300 °C before activation had Qe of 9.08 mg/g and Ef of 38.66%.

Artificial neural networks (ANNs) are frequently employed in heat exchanger analysis and optimization due to their improved predictive accuracy and their ability to optimize processes. Artificial neural networks (ANNs) model heat exchanger systems well due to their complex, nonlinear input-output interactions. Abo *et al*[22] Studies show that this knowledge improves forecasts and optimization of heat exchanger performance. Simulating operational variables with artificial neural networks predicts heat exchanger performance. ANNs and GAs are frequently used for heat exchanger enhancement. Building and training artificial neural networks (ANNs) improves heat exchanger design and analysis, but it takes expertise and processing power. ANN complicates GA and CFD, but heat exchanger performance and efficiency improve. Methods should fit application limitations. Acid centrifugation enhanced clarity efficacy to 66.17 wt%. % CaO at 100 °C, 50 °C, and 3.50 pH by Apo *et al*. The 65.94 wt% CaO decline matched the model's highest projection. A GA optimization lowered sugarcane molasses CaO by 66.21 wt%, while an ANN enhanced the prediction model with 0.99866 R-squared. GA optimization improved the process. Bai *et al*.[23] compared bow-shaped vortex generators to finned-tube heat exchangers. ANN and GA were used to improve vortex generator form and forecast accuracy. The Nusselt number and friction factor were used to measure the hydrodynamic and thermal performance. They examined hydraulic and thermal performance simultaneously using the relative efficiency index. Heeraman *et al*.[24] modeled 14,000 Reynolds twin-pipe heat exchangers in ANSYS 16.0. For ANN model testing, we mimicked tubes with twisted tapes and dimples, with specified sizes and twist ratios. Nusselt and friction factors were calculated for dimpled twisted tape insert tubes. The validation approach predicts 0.08% inaccuracy, 2.1% friction, and Nusselt values below 3.30% for the experimental data. Jradi *et al*.[25] found that RSM was more accurate than the other two methods. RSM accurately predicts heat exchanger fouling resistance, with an R-squared value of 0.9998, MSE of 5.9388 × 10^-13, and RMSE of 7.7064 × 10^-7. The RSM optimization technique achieved optimal values of 114.805 hours, 72.214 °C for the acid input, 80.407 °C for the acid output, 116.784 °C for the steam temperature, 1642.47 kg/m^3 for the acid density, and 2308.1 m^3/h for the volume flow rate. Data-predicted fouling resistance differs by 2.19%. Barhatte *et al*.[26] found that reducing the hydraulic diameter improves heat transfer in microchannel heat exchangers but increases pumping power and pressure loss, and pumping force and hydraulic heat transport benefit from 0.001 m nozzles. The study shows a 0.9% uncertainty in the Nusselt-Prandtl (Nu-Pr) connection, confirming analytical and numerical approaches. In virtual laboratory and heat exchanger tests by Al-Rawashdeh *et al*.[27] the ANN model and regression-based predictions match the experiments within 3%. This lets students connect to the content without a lab. Virtual lab results are usually confusing. Documentation may explain ANN's realistic virtual lab. Virtual labs teach heat exchange and imitate real-world situations. Naphon and colleagues' research[28–32] was the most successful. They used an artificial neural network to study the heat transfer of spirally fluted tubes,[28] micro-channel heat sinks,[29] air-cooling rubber mattresses for the elderly and bedridden,[30] square tubes with oscillating electromagnetic fields,[31] and spirally coiled tubes with electromagnetic.[32] Future research on heat exchanger dynamics and energy exchange should benefit from this model.

A lot of thermal system research uses ANN. In AI, data analysis, and machine learning, artificial neural networks are essential. Here are several major benefits: Because they accurately model complex, nonlinear input-output interactions, ANNs are valuable in many applications. Noise and missing data are no problem for automatic neural networks. Learning predictive models with artificial neural networks (ANNs) can be applied to new data. Parallel computing could speed up the processing of large datasets by ANNs. Machine learning algorithms, such as ANNs, can discover patterns and structures in data. The efficiency with which artificial neural networks (ANNs) processed increasingly sophisticated models and larger datasets helped drive the development of big data applications. Programmable ANNs can learn and adapt to new data and scenarios.

ANNs were employed in thermal system research. ANNs aid AI, data science, and machine learning. Key benefit: Artificial neural networks (ANNs) have many applications because they can model complex, nonlinear input-output relationships. Fuzzy and missing data help ANNs. ANN prediction models can use training data on new data. Parallel processing could help ANNs with large datasets. ANNs automatically find data patterns and structures, simplifying modeling. For big data, ANN can handle more sophisticated models and datasets. Programmable ANN automatons adapt to fresh information. A neural network optimizes the drying of water hyacinth. Data processing determined the water hyacinth's moisture ratio, starting and ending operation times, and size measurements. The ANN compared experimental outcomes.

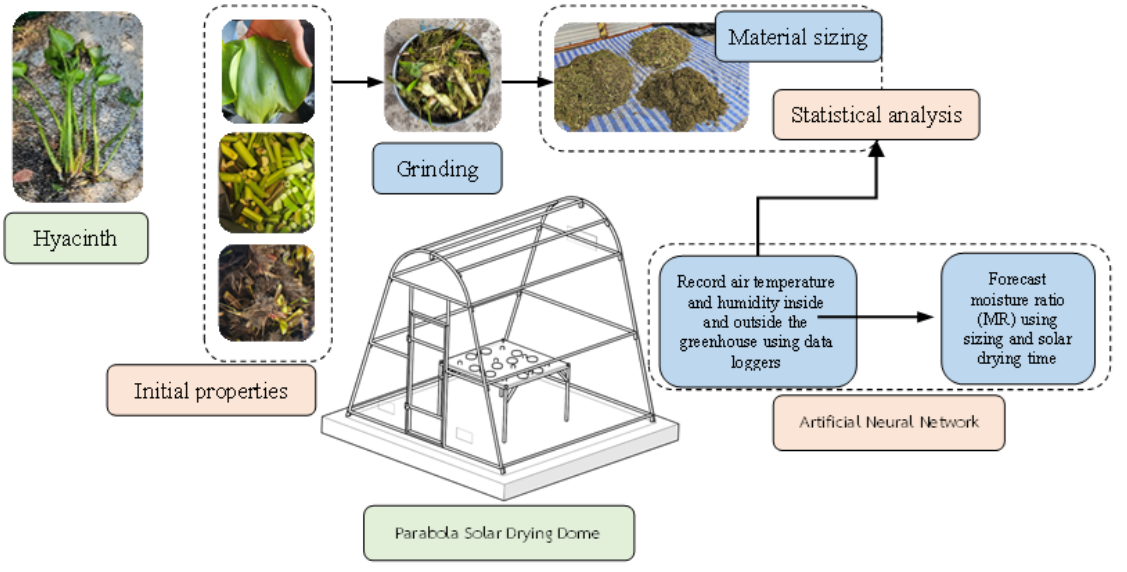

Fig. 1: Schematic diagram of the present experimental system.

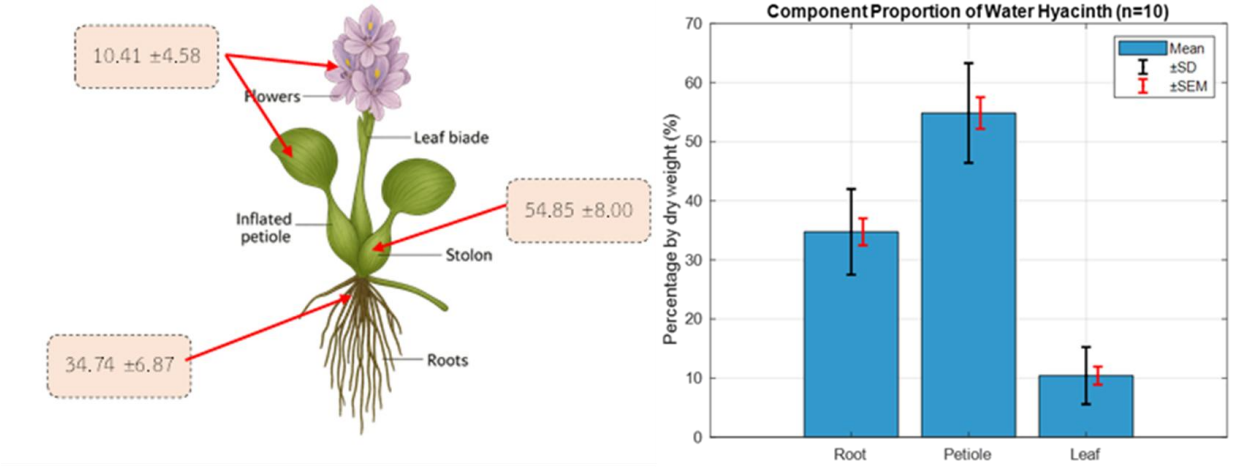

Fig. 2: Component of hyacinth.

2. Materials and methods

2.1 Solar drying dome and controlled system

As shown in Fig. 1, the solar drying dome is 3000 mm long, 3000 mm wide, and 2700 mm tall. The dryer frames use a 20 mm x 20 mm aluminum profile. The metal framework is protected by 200-millimeter translucent acrylic. The solar drying dome's middle zone has an 800 mm × 1200 mm platform and wire mesh for water hyacinths. Two 25-watt motors power the suction fans on top of the door. A humidity transmitter on the fan emits an alarm when the relative humidity difference between inside and outside air exceeds a particular threshold. Following this examination, the fan's speed and direction are modified. The self-closing loop in greenhouse solar dryers regulates drying processing parameters.

2.2 Materials

One of several weeds that rapidly spread in marshes is water hyacinth, which causes environmental problems. Water hyacinth must be used in plywood manufacturing in this research. This study examines the heating properties of water hyacinth as a biomass fuel at different moisture levels. Experimental drying conditions were tested in Nakhon Ratchasima Province, Thailand, at 15 ° E in winter 2025 to determine the optimal conditions for using water Hyacinth in plywood. Design, construction, and testing of the solar drying dome with an automatic closed-loop control system for water Hyacinth drying. Water Hyacinth from Nakhon Ratchasima, Thailand, was employed in the study. According to Fig. 2, the water Hyacinth base and root had a mass of 34.74 ±6.87%, the stem 54.85 ±8.00%, and the leaf 10.41 ±4.58%. At the start, the humidity was 84.67 ± 2.67 Mwb and 570.00 ± 102.96 Mdb. The three groups that have been chopped down are named massive scale (L), medium scale (M), and small scale (S) for water hyacinths that have been cut once, twice, and three times, respectively, as illustrated in Fig. S1.

2.3 Statistical analysis

The moisture ratio (MR) was calculated over 24 hours using a solar parabolic dome to monitor weight decrease. It also

measured temperature and relative humidity inside and outside the greenhouse to study the drying process. ANOVA, Levene's test, and Tukey's HSD test were used to compare material groups' properties and determine statistical significance.

3. Artificial neural networks approach

3.1 General of artificial neural network

Machine learning (ML) enables AI to create data-driven models and algorithms without human programmers. Data can teach computer-based researchers and engineers the input/output model for forecasting or classifying incoming data. In ML, ANNs are popular supervised learning models. Layers of data help it tackle complex scenarios. In unsupervised learning, ANN models learn input-output relationships from training datasets. A neural network has input, hidden, and output layers. Read about ANN models.[33] AI neural networks (ANN) fascinate. Constructing ANNs is difficult due to their complex structure and parameter settings.

Artificial neural network-based nonlinear mathematical models are simple, powerful, user-friendly, and versatile; hence, their use is rising. Researchers in this study used an artificial neural network. Artificial neural networks are more accurate than conventional algorithms, can learn from new data, and represent complex relationships. Their pattern recognition skills help them excel at picture and voice recognition. Learning from big datasets, ANNs generalize well to new data. Neurons output parameters using connection weights from other neurons. An evolutionary method indicated the number of buried nodes and which newly picked critical attributes to prioritize. Ridge regression is functional for nonlinear regression. First is better numerically. By incorporating bias variables X and weights, the Levenberg-Marquardt method backpropagates to determine the performance Jacobian 'jX'. Use Levenberg-Marquardt for nonlinear least squares. Gauss-Newton and gradient descent compromise. This method works well for optimization and curve-fitting tasks that involve iteratively adjusting parameters to minimize the difference between expected and observed values.

ML, engineering, and statistics employ this approach. Each variable is changed by this approach.[33] On a coordinate plane, straight-line linear functions activate the output layer. To express the line's slope and y-intercept, use y = mx + b. The y-axis intersects with steep slopes and y-intercepts. Science, engineering, and economics employ linear functions to model relationships between variables. Transforming side ratios into triangle angles using principal trigonometric functions, such as the tangent function, activates the buried layer. One right triangle side is proportional to the adjacent angle's tangent. As tan(θ) = opposing/adjacent, the tangent function represents the opposite or neighboring angle. The tangent function has a periodic nature, repeating its values every π radians for a period of π. Periodic process modeling, physics, computer graphics, and engineering require it. Backpropagation determines inaccuracy during training. To train and test neural networks, the input data must have a structure and a goal. Training and validation datasets use the same data. Changes to biases and weights can improve input-output alignment.

3.2 ANN performance analysis

Test the enhanced ANN model's anticipated outcomes performance to analyze the findings. Using the correlation coefficient (R) and mean square error (MSE),[34] we can identify ANN models that are accurate during training and predictions Eq. (1).

$$R = \frac{cov(a,p)}{\sqrt{cov(a,a)\cdot cov(p,p)}} \quad (1)$$

where *cov(a, p)* is the covariance between the sets *a* and *p*, the measured data and predicted outcomes as follows Eq. (2-3):

$$cov(a,p) = E\left[(a-\mu_a)(p-\mu_p)\right] \quad (2)$$

$$cov(a,a) = E[(a-\mu_a)^2] \quad (3)$$

where E represents the expected value, whereas μ_a and μ_p represent the mean values of a set and p sets, respectively. Furthermore, *cov(a, a)* and *cov(p, p)* represent the auto-covariances of the *a* and *p* sets, respectively.

The MSE[34] can be determined from:

$$MSE = \frac{1}{N}\sum_{i=1}^{N}(a_i - p_i)^2 \quad (4)$$

where a_i and p_i represent the measured data and predicted results for the i-th set, respectively, and N denotes the total number of datasets.

4. Results and discussion

4.1 Experimental results

Fig. 3 compares greenhouse and outside air temperatures. The greenhouse's interior and exterior air temperatures differed dramatically during the test. Especially between 13:00 and 15:00, when the interior temperature peaks at 46°C and the outside temperature is 37 °C. Greenhouse drying and environmental control effectiveness can be affected by the maximum temperature differential of 10 °C. Fig. 4 illustrates that during daylight hours, the greenhouse's relative humidity (%RH) is much lower than the external value. Outdoor humidity is 75–80% from 11:00 to 17:00.

Meanwhile, the interior has diminished by 50-55%. The temperature increase within the closed system causes a maximum humidity variation of more than 25%. This enables more efficient moisture drainage. This data shows that greenhouses can efficiently control humidity during periods of high sunlight, making it an ideal opportunity to employ solar energy for drying or other operations that require dryness within the system.

Fig. S2 illustrates the tiny, medium, and large scales of dry hyacinths. Fig. 5 shows how moisture ratios vary with operating time for Hyacinths of different sizes. The

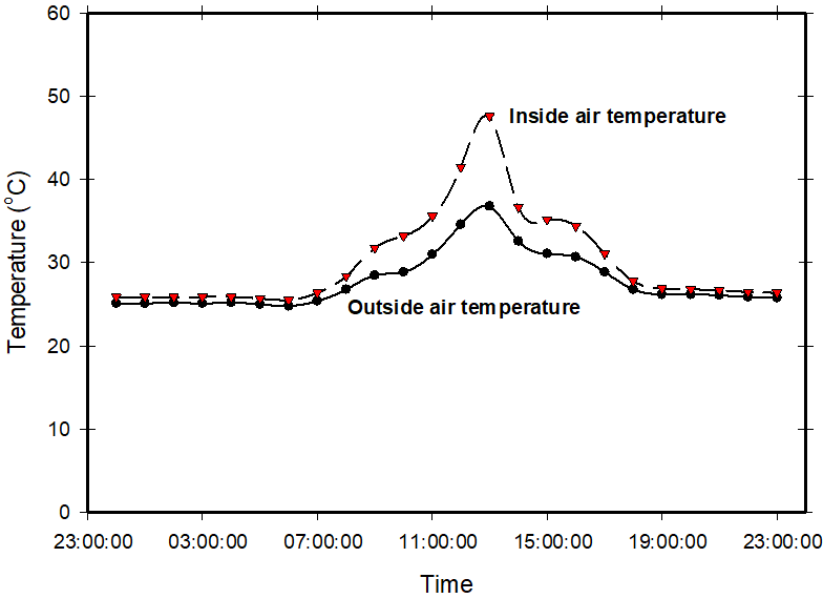

Fig. 3: Variation of the temperature inside and outside the greenhouse.

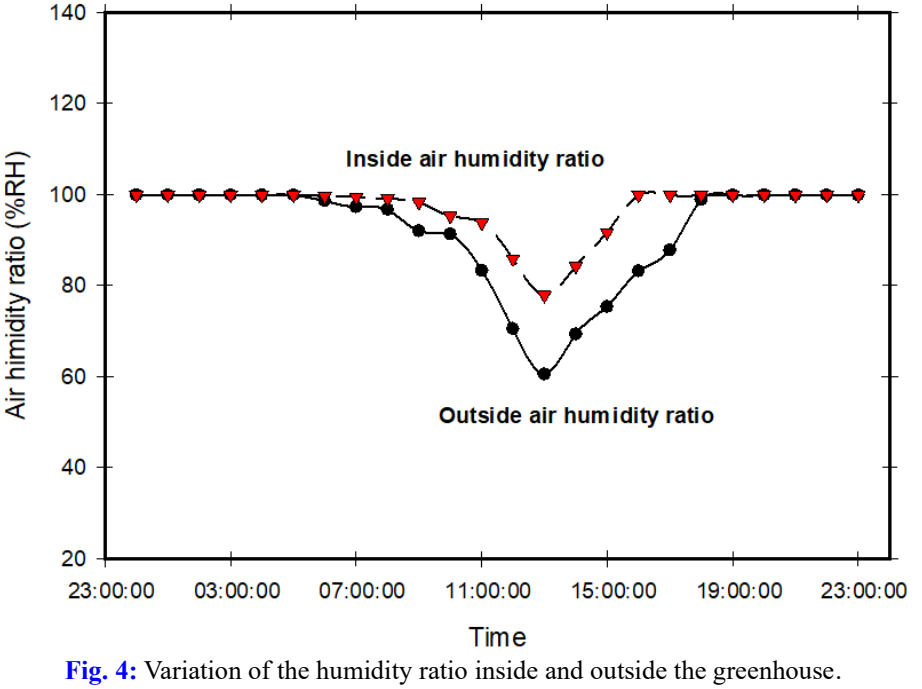

Fig. 4: Variation of the humidity ratio inside and outside the greenhouse.

association between the moisture ratio (MR) and the dehumidification period of the three hyacinth sizes, S, M, and L, was discovered to be consistent with the drying process mechanism, which involves the evaporation of water from a material when heated. However, the rate of MR reduction varies significantly depending on the substance. The large group (L) had a faster decrease in MR values than the M and S groups in the early stages and maintained the lowest levels throughout the experiment. This could be due to the larger material's higher cavitation. This makes water evaporation easier. Group M declines at a moderate rate, whereas Group S shows the slowest moisture decline, remaining consistently higher than the other groups over the same period. This increases the adherence of particles or crust on the material's surface, reducing water evaporation inside the greenhouse.

4.2 Statistical analysis

In this study, it is necessary to use more miniature water hyacinths to produce plywood. As a result, the water hyacinth is reduced in size using a blade grinder. The three groups that have been chopped down are named massive scale (L), medium scale (M), and small scale (S) for water hyacinths that have been cut once, twice, and three times, respectively. Density testing was performed utilizing liquid substitution in accordance with ISO 17892-2:2014, beginning with the manufacture of dried water Hyacinth samples until they were fully moisture-free. The sample is weighed for dry weight (Ws) and then dipped in a container containing toluene or

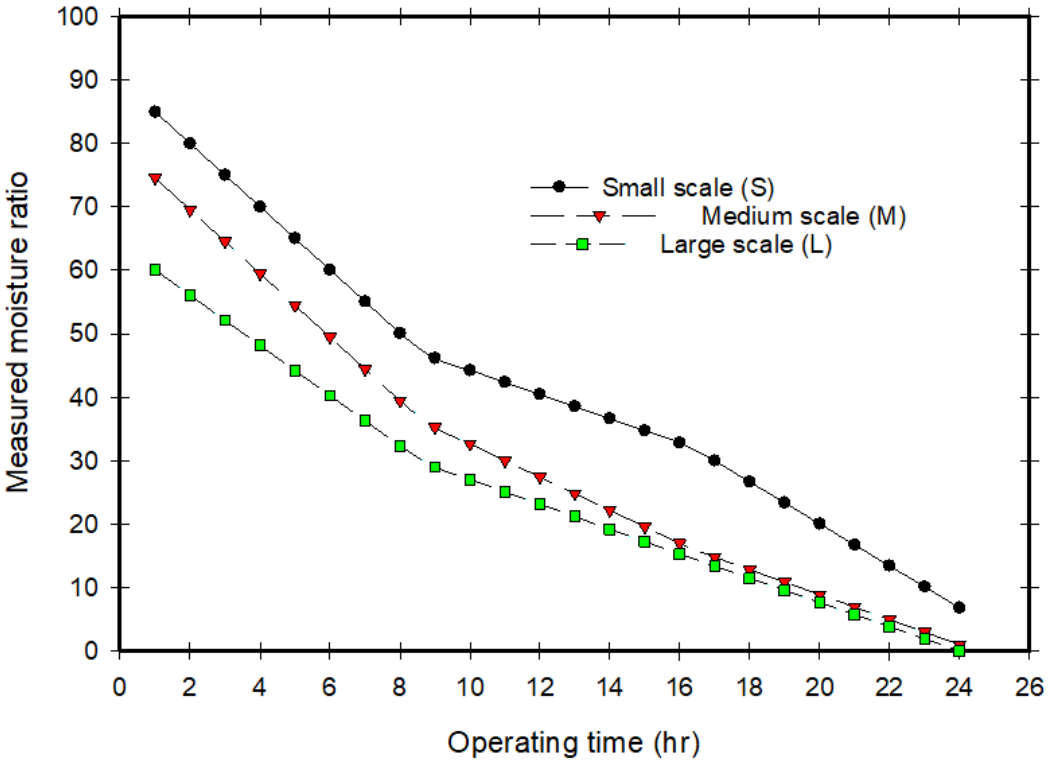

Fig. 5: Variation of moisture ratio with operating time for different-sized scale hyacinths.

Table 1: Density of different-sized scales of hyacinth.

Size scale	Mean	SD	SEM	95% Confidence Interval for Mean		Minimum	Maximum
				Lower Bound	Upper Bound		
S	439.32	42.36	24.45	334.10	544.54	401.12	484.87
M	329.12	2.54	1.47	322.80	335.45	326.19	330.59
L	290.92	11.66	6.73	261.95	319.89	282.11	304.15
Total	353.12	70.27	23.42	299.11	407.13	282.11	484.87

Table 2: Homogeneity of variances test.

Levene's Test Criteria	Levene Statistic	df1	df2	Sig.
Based on Mean	4.588	2	6	0.062
Based on Median	2.179	2	6	0.194
Based on Median and with adjusted df	2.179	2	2.511	0.283
Based on the trimmed mean	4.402	2	6	0.067

paraffin, which will not react with or penetrate the fibers. Measure the volume of the displaced liquid (V) by raising the liquid level in the container, then divide the dry weight value by the displacement volume to determine the density value (Eq. (5)), as shown in Table 1.

$$\rho = \frac{W_s}{V} \tag{5}$$

Table 2 displays the results of the Levene test for homogeneity of variances, along with the significance level (Sig.). The p- value obtained from the mean was 0.062, which was greater than 0.05, suggesting that there was no statistically significant difference in variance among the groups. As a result, the hypothesis is that when the variance is homogeneous, ANOVA is appropriately used.

The ANOVA analysis, as shown in Table 3, compared the density of water Hyacinths across groups of different sizes, yielding an F value of 27.595 and a Significance threshold of 0.000. (p-value) of 0.001, which was less than the significant threshold of 0.05. The average density of the three water hyacinth sizes was statistically significant. It may be determined that the material's size influences the density value,

and further study should be performed using the Post Hoc method to determine whether pairs of groups are statistically distinct.

Table 3: ANOVA analysis of hyacinth density.

	Sum of Squares	df	Mean Square	F	Sig.
Between Groups	35625.360	2	17812.680	27.595	.001
Within Groups	3872.980	6	645.497		
Total	39498.340	8			

Table 4 presents a comparison of hyacinth density across size groups using the Post Hoc Tests by Tukey HSD and LSD. Comparisons between the size groups "S" and "M" and between "S" and "L" yielded Sig values < 0.05 in both approaches, indicating a statistically significant difference. Neither in terms of the average nor the 95% confidence interval. While the groups "M" and "L" have a value of Sig. = 0.235, which is more than 0.05, there is no significant difference.

Table 4: Post Hoc Test with Tukey HSD and LSD methods.

Test type	Mean Difference (I-J)		Sig.
Tukey HSD	S	110.1977*	0.004
		148.3996*	0.001
	M	-110.1977	0.004
		38.2019	0.235
	L	-148.3996	0.001
		-38.2019	0.235
LSD	S	110.1977*	0.002
		148.3996*	0.000
	M	-110.1977	0.002
		38.2019	0.115
	L	-148.3996	0.000
		-38.2019	0.115

When the mean difference was calculated, the "S" group had an average density value that was 110.20 units greater than the "M" group and 148.40 units higher than the "L" group. In comparison, the difference between "M" and "L" was only 38.20 units, which was insufficient to yield a statistically significant result. As a result, reducing hyacinth size to the "S" level leads to a large increase in density values. Meanwhile, the difference between the "M" and "L" groups is not statistically significant so they can be combined based on density. This discovery is critical for the design of processing procedures or for separating raw Hyacinth sizes to achieve physical qualities acceptable for use.

Table 5 shows that shredding reduces the material's size, thereby affecting its density. The small group "S" has a maximum average density of 439.32 ± 42.36 g/cm^3, which is statistically different from the other groups. The medium "M" and large "L" groups had average values of 329.12 ± 2.54 and 290.92 ± 11.66 g/cm^3, respectively. This demonstrates that there are two groups. There was no statistical difference; however, a significant difference was observed in the small group.

Table 5: Mean density of Hyacinth with statistical comparison (Tukey HSD, $\alpha = 0.05$).

Size scales	Density (g/cm^3) ± SD
S	439.32 ± 42.36
M	329.12 ± 2.54
L	290.92 ± 11.66

*__Note:__ Means followed by the same letter within the column are not significantly different at the 0.05 level according to Tukey's HSD test.

4.3 Artificial neural network analysis

ANN is a mathematical model based on how the human brain's nervous system functions. The goal is to make the system capable of effectively learning from data, experiments, or examples. An artificial neural network (ANN) consists of layers of neurons, also called artificial neurons. This is related to a network that connects the input layer, which accepts input data and passes it via one or more hidden layers that process complicated relationships in the data, to the output layer, which provides the final result. Each neuron in the network takes input from the previous neuron, multiplies it by the weight, and then passes the result through the activation function to generate a value transmitted to the next layer. During the learning phase, the ANN compares the calculated results to the actual data values. It then updates the weights using backpropagation, thereby minimizing error and improving prediction accuracy.

The ANN has a single hidden layer with the structure depicted in Fig. 6, which uses the hyperbolic tangent sigmoid(Tansig) activation function. The implementation of Tansig in the hidden layer allows the network to learn complex, nonlinear patterns in the data more efficiently, since this function can convert linear values into nonlinear ones, which is required for learning complex data. The neural network utilized can generate equations such as those illustrated in Eq. (6–11).

$$x = [x_1, x_2] \tag{6}$$

$$\hat{y} = f_2(W_2 \cdot f_1(W_1 \cdot x + b_1) + b_2) \tag{7}$$

$$\hat{y} = net(x) = [\hat{y}_1, \hat{y}_2, \hat{y}_3] \tag{8}$$

$$f_1(z) = tanh(z) \tag{9}$$

$$f_2(z) = z \tag{10}$$

$$f_3(z) = z \tag{11}$$

where x_1 is the operating time
x_2 is the size scale
$\hat{y}_1$ is the predicted moisture ratio for "S"
$\hat{y}_2$ is the predicted moisture ratio for "M"
$\hat{y}_3$ is the predicted moisture ratio for "L"
W_i is the weight of i hidden layer
b_i is the bias of i hiden layer

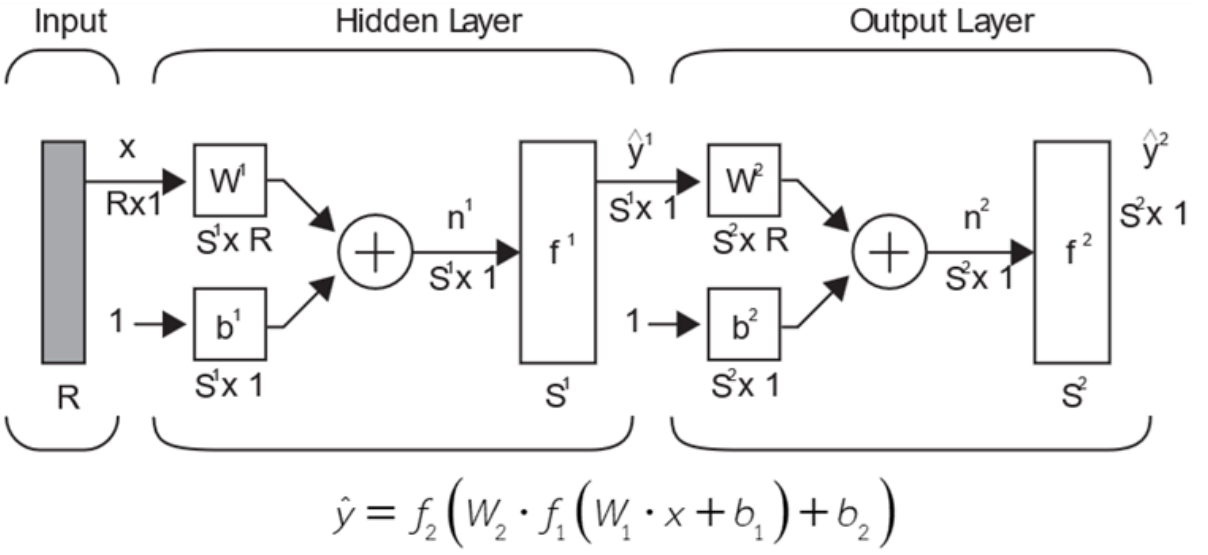

Fig. 6: The proposed artificial neural network used in the present study.

Data training employs the Levenberg-Marquardt algorithm, which combines the benefits of two major optimization methods: Gradient Descent, which is suitable for determining the minimum of a nonlinear function by moving in the direction of decreasing slope but is slow to approach the minimum, and Gauss-Newton. It has a faster approach velocity to the minimum value, but it is limited when the function is highly nonlinear or the data is extremely noisy.

Adjusting the number of neurons from 1 to 10 allows us to test the R-squared value (maximum). The data is conveyed from the two hidden layers to the output layer, which consists of two neurons and uses the Purelin (linear activation function), which maintains values that are generally constant. The model's input parameters—the toggling status of the water Hyacinth size scales and operation time—are suitable for regression forecasting. The moisture ratio of the Hyacinth is the output parameter. A conventional sensitivity analysis is conducted to identify an appropriate model. To begin training, the algorithm randomly partitions the data into training, validation, and test sets using the K-fold approach. This ensures that the data division procedure is randomized. This method reduces bias caused by data ordering and its impact on model learning by ensuring the model receives inputs that are evenly distributed. The datasets are split into three categories: 70% for training, 15% for validation, and 15% for testing.

Fig. 7 illustrates the relationship between the number of nodes in the ANN's hidden layer and the model's accuracy. When the hidden layer has only one node, the R^2 value is around 0.297, indicating that the model cannot adequately capture the data. There is a critical turning point at two nodes that allows the model to begin learning successfully, and the performance remains consistent even with more nodes. This indicates that the model is stable. Choosing the appropriate number of nodes, such as 3–5. This enables the model to be highly economical while still calculating quickly and avoiding overfitting, making it suitable for real-world applications like automatic drying control using sensors or embedded devices.

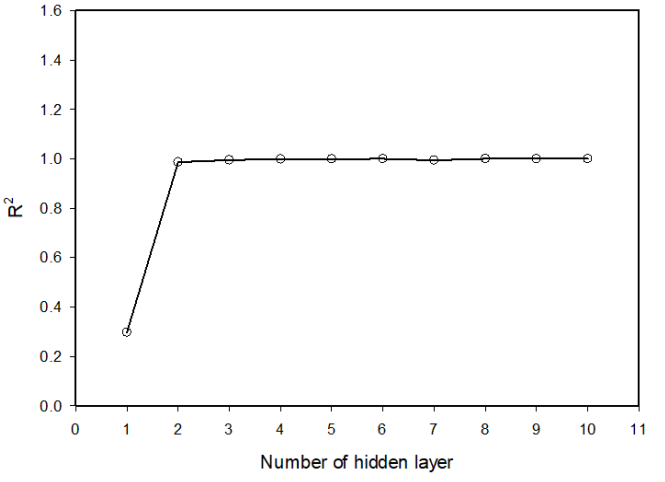

Fig. 7: Variation of R^2 over the number of hidden layers.

Fig. 8 depicts the link between the number of nodes in the hidden layer and the ANN's mean squared error (MSE) in predicting hyacinth moisture ratios (S). After three or more nodes, the error value decreases significantly to less than 10. A low static error number (around zero) suggests much higher accuracy. As a result, it is best to choose the most appropriate number of nodes, such as 4 or 6, to balance the model's accuracy and practicality successfully. Fig. S3 compares the measured moisture ratio of Hyacinth "S" with the projected moisture ratio for various hidden layers (1-5 node range). It was found that the model with more nodes better learned and forecasted the dehumidification trend, in line with the experimental data. Especially during the 3-5 node range, which produces precise and consistent findings. However, using only one node prevents the model from learning any patterns. As a result, the projected value remains constant at all times. While adding more nodes than six yields more accurate results, there is evidence of overfitting, particularly in the late stage, when some moisture ratio values become negative, contradicting the physical reality of the drying process.

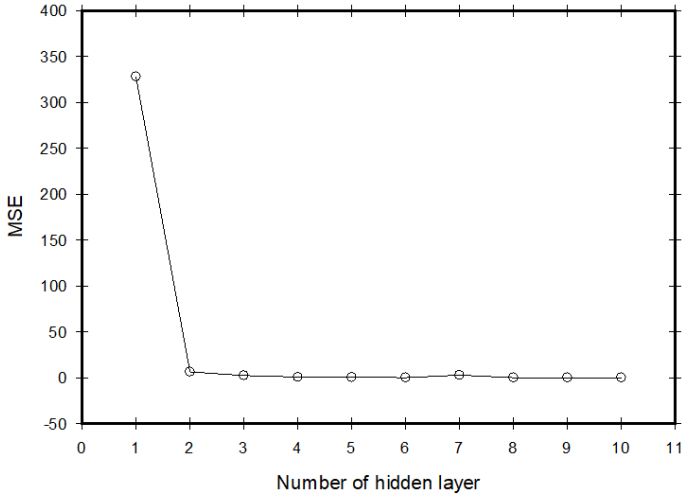

Fig. 8: Variation of mean squared error over many hidden layers.

Fig. S4 depicts the forecast results for "S", "M", and "L" hyacinths over 24 hours. Models with more nodes showed a better overall trend in learning to decrease the fraction of moisture. Compared to the experimental data, the model with two or more hidden layers exhibits a more realistic downward trend in the moisture ratio. The number of hidden layers consistently predicted a value of around 23.29 over time; however, the number of nodes between 3 and 5 showed a more consistent pattern at the beginning, middle, and conclusion of the period. While the number of nodes greater than 6 still produces a similar prediction value, the prediction value tends to decline too quickly at times, which may indicate the onset of minor overfitting, particularly after the 20th hour. As a result, taking into account both the model's overall accuracy and stability, the forecast is lower than the actual data. The best number of nodes for medium-sized hyacinths is 5-6 nodes, which strikes a decent balance between learning and maintaining data features.

5. Uncertainty from this study

This study's uncertainty comes from experimental drying measurements and predictive ANN modeling. Mass, temperature, and relative humidity measurements during water hyacinth drying in the solar parabolic dome are the main experimental uncertainties. The moisture ratio (MR) is computed from repeated mass measurements over 24 hours, but scale precision, ambient variables, and sample handling can cause mass readings to vary. Temperature and humidity sensors within and outside the greenhouse add uncertainty due to instrument resolution, calibration drift, and time-response lag when solar intensity rapidly varies. The drying rate and MR trend are further influenced by the difference between inside and external humidity, an important fan parameter.

ANOVA, Levene's test, and Tukey HSD assess hyacinth size group differences to eliminate uncertainty. The very significant ANOVA F-value proves that density and moisture behavior differences are not random, whereas the non-significant Levene's test verifies variance homogeneity, lowering statistical uncertainty. This boosts experimental trend confidence.

In ANN modeling, model training and forecast accuracy are unknown. The dataset was randomly partitioned into training, validation, and testing subsets using a K-fold technique to reduce data ordering bias. ANN's correlation coefficient (R^2) and mean squared error (MSE) measure predicting uncertainty. High R^2 values (>0.99) and low MSE (<1.0) suggest very little prediction uncertainty. The study also finds overfitting uncertainty, especially when too many hidden nodes create unrealistic negative predictions at late drying times. If uncontrolled, model complexity can increase uncertainty. Choosing 4–6 hidden nodes balances learning capacity and generalization accuracy, reducing this danger.

6. Conclusion

In a solar parabolic drying system, small hyacinths demonstrated the greatest average density of 439.32 g/cm³. Hyacinths of medium and large sizes have similar values. The ANOVA and Tukey HSD tests indicated that the density of the "S" group differed significantly from that of the other two groups. There was no statistical difference between the "M" and "L" categories. This permits them to be physically placed in the same group. Under drying conditions, all three hyacinth sizes dehumidified in solar parabolic greenhouses showed a consistent pattern of decreasing moisture ratios over time. One explanation for the slower dehumidification rate in the smaller group could be the formation of a crust on the material's surface during baking, or a more compact interior fiber structure, both of which would delay water evaporation from the material. The larger group, on the other hand, has the fastest dehumidification rate. Material size has a direct relationship with dehumidification efficiency. Create a neural network model to estimate the moisture ratio based on experimental data on time and hyacinth size scale. Using an ANN with 4-6 hidden layer nodes resulted in an R^2 value of more than 0.99 and an MSE value lower than 1.0, indicating significant accuracy in learning and forecasting the moisture ratio.

Acknowledgments

This research project is supported by Science Research and Innovation Fund. Agreement No. FF68/125.

Conflict of Interest

According to the authors, there are no known competing financial interests or personal links that may have influenced any of the material provided in this study.

Data availability statement

The data supporting this study's findings are available from the corresponding author upon reasonable request.

Supporting Information

Applicable.

CRediT Statement

J. Jongpluempiti and **P. Vengsungnle:** Conceptualization, Methodology, Data curation, Formal analysis, Software. **S. Poojeera:** Conceptualization, Methodology, Data curation. **A. Srichat:** Conceptualization, Methodology, Data curation. **A. Siricharoenpanich:** Data curation, Formal analysis, Original draft, Writing – Review and editing. **P. Naphon:** Data curation, Formal analysis, Software, Writing – Original draft, Writing – Review and editing. All authors affirm their shared responsibility and commitment to be accountable for all facets of the research work.

References

[1] R. Mukherjee, M. Ghosh, B. Nandi, Improvement of dry matter digestibility of water hyacinth by solid state fermentation using white rot fungi, *Indian Journal of Experimental Biology*, 2004, **42**, 837–843.

[2] I. C. O. Akendo, L. Gumbe, A. N. Gitau, Dewatering and drying characteristics of water hyacinth (Eichhornia Crassipes) petiole, *Part II. Drying Characteristics*, *Agricultural Engineering International: The CIGR Journal*, 2008, **4**, 1-13.

[3] S. H. Hasan, D. Ranjan, M. Talat, Water hyacinth biomass (WHB) for the biosorption of hexavalent chromium: Optimization of process parameters, *BioResources*, 2010, **5**, 563-575, doi: 10.15376/biores.5.2.563-575.

[4] O. A. Ighodalo, Z. Zoukumor, C. Egbon, S. Okoh, K. Odu, Processing water hyacinth into biomass briquettes for cooking purposes, *Journal of Emerging Trends in Engineering and Applied Sciences*, 2011, **2**, 305–307.

[5] E. V. Casas, J. G. Raquid, K. F. Yaptenco, E. K. Peralta, Optimized drying parameters of water hyacinths (Eichhornia crassipes. L), *Science Diliman*, 2012, **24**, 28–49.

[6] B. Weng, J. Zhou, S. Zheng, X. Chen, W. Zhang, Q. Huang, Field utilization of dried water hyacinth for phosphorous recovery from source-separated human urine, *Journal of Environmental Protection*, 2012, **3**, 715-721, doi: 10.4236/jep.2012.38085.

[7] M. I. Shoughy, A. F. Abdraboh, A. B. El-Nagar, Drying behaviors of water hyacinth by multi-tray solar dryer, *Egyptian Journal of Agricultural Research*, 2014, **92**, 273-288, doi: 10.21608/ejar.2014.154828.

[8] S. Rezania, M. Ponraj, M. F. M. Din, A. R. Songip, F. M. Sairan, S. Chelliapan, The diverse applications of water hyacinth with main focus on sustainable energy and production for new era: an overview, *Renewable and Sustainable Energy Reviews*, 2015, **41**, 943-954, doi: 10.1016/j.rser.2014.09.006.

[9] A. Jongmeesuk, V. Sanguanchaipaiwong, Pretreatment and Enzymatic Hydrolysis from Water Hyacinth (Eichhornia crassipes), *KMITL-Science and Technology Journal*, 2015, **14**, 80-86.

[10] N. Mukaratirwa-Muchanyereyi, J. Kugara, M. F. Zaranyika, Adsorption of volatile polar organic solvents on water hyacinth (Eichhornia crassipes) root biomass: thermodynamic parameters and mechanism, *International Journal of Environmental Science and Technology*, 2016, **13**, 1941-1950, doi: 10.1007/s13762-016-1016-1.

[11] Ismiyarto, Ngadiwiyana, T. Windarti, R. S. Purbowatiningrum, M. Hapsari, F. H. Rafi'ah, Suyanti, M. S. Haq, Synthesis of furfural from water hyacinth*(eichornia croassipes)*, *IOP Conference Series: Materials Science and Engineering*, 2017, **172**, 012027, doi: 10.1088/1757-899x/172/1/012027.

[12] S. Sukarni, A. E. Widiono, S. Sumarli, R. Wulandari, I. M. Nauri, A. A. Permanasari, Thermal decomposition behavior of water hyacinth (*eichhornia crassipes*) under an inert atmosphere, *MATEC Web of Conferences*, 2018, **204**, doi: 10.1051/matecconf/201820400010.

[13] W. Rahmawati, A. Haryanto, S. Suharyatun, Development of biodegradable board using water hyacinth (eichornia crassipes), *International Journal of Environment, Agriculture and Biotechnology*, 2018, **3**, 170-174, doi: 10.22161/ijeab/3.1.21.

[14] R. D. Yetti, R. Junita, Manufacture and characterization of microcrystalline cellulose of water hyacinth (Eichhornia Crassipes (Mart.) Solms) by enzymatic process, *International Journal of Research*, 2020, **7**, 384–389, doi: 10.4444/IJRR.1002/2131.

[15] K. Amante, L. Ho, A. Lay, J. Tungol, A. Maglaya, A. Fernando, Design, fabrication, and testing of an automated machine for the processing of dried water hyacinth stalks for handicrafts, *IOP Conference Series: Materials Science and Engineering*, 2021, **1109**, 012008, doi: 10.1088/1757-899x/1109/1/012008.

[16] R. G. P. Rajan, S. E. Jona, S. Dhinakaran, J. Dinesh, R. Deepika, S. Aruna, D. Manikandavelu, Water hyacinth a sustainable source of feed, manure and industrial products: a review, *Agricultural Reviews*, 2022, **44**, 389-392, doi: 10.18805/ag.r-2181.

[17] N. Hoc Thang, Treatment of water hyacinth fibers to improve mechanical and microstructural properties of green composite materials, *Sigma Journal of Engineering and Natural Sciences – Sigma Mühendislik Ve Fen Bilimleri Dergisi*, 2022, **40**, 292-299, doi: 10.14744/sigma.2022.00033.

[18] H. T. Nguyen, T. B. H. Nguyen, Treatment of water hyacinth fibers to improve mechanical and microstructural properties of green composite materials, *Nano Hybrids and Composites*, 2022, **35**, 111-122, doi: 10.4028/p-30xboe.

[19] B. D. Wembe, R. Djomi, N. Konai, G. E. Ntamack, F. A. Tsopmo, O. E. Olubusoye, L. Meva'a, Investigation on the mechanical properties of paper water hyacinth (eichhornia crassipes), *European Journal of Engineering and Technology Research*, 2023, **8**, 54-58, doi: 10.24018/ejeng.2023.8.1.2965.

[20] N. Prongmanee, A. Noulmanee, R. Dulyasucharit, S. Horpibulsuk, J.-C. Chai, Durability against wetting and drying cycles and installation damage of water hyacinth geotextiles coated with natural rubber latex, *Journal of Materials in Civil Engineering*, 2023, **35**, 04023408, doi: 10.1061/jmcee7.mteng-15721.

[21] R. Rosidah, S. Sri Rahayu, E. Susanti, Removal of cadmium (II) by adsorption using water hyacinth (*Eichhornia crassipes*) dried biomass, *Journal of Ecological Engineering*, 2023, **24**, 246-253, doi: 10.12911/22998993/156692.

[22] L. D. Abo, S. M. Hailegiorgis, M. Jayakumar, S. Venkatesa Prabhu, G. T. Gindaba, A. S. Hamda, B. S. Naveen Prasad, RSM-, ANN-, and GA-based process optimization for acid centrifugation treatment of cane molasses toward mitigating calcium oxide fouling in ethanol plant heat exchanger, *International Journal of Chemical Engineering*, 2024, **2024**, 2744213, doi: 10.1155/2024/2744213.
[23] Z. Bai, A. M. Abed, P. K. Singh, D. Abduvalieva, S. Alkhalaf, Y. Elmasry, A. Alruwaili, F. S. Alharbi, F. Riaz, Bow-shaped vortex generators in finned-tube heat exchangers; ANN/GA-based hydrothermal/structural optimization, *Case Studies in Thermal Engineering*, 2024, **55**, 104135, doi: 10.1016/j.csite.2024.104135.
[24] J. Heeraman, R. Kumar, P. K. Chaurasiya, T. N. Verma, D. K. Chauhan, Optimisation and comparison of performance parameters of a double pipe heat exchanger with dimpled twisted tapes using CFD and ANN, *Proceedings of the Institution of Mechanical Engineers, Part E: Journal of Process Mechanical Engineering*, 2025, **239**, 3251-3268, doi: 10.1177/09544089231223599.
[25] R. Jradi, C. Marvillet, M. R. Jeday, Multi-objective optimization and performance assessment of response surface methodology (RSM), artificial neural network (ANN) and adaptive neuro-fuzzy interfence system (ANFIS) for estimation of fouling in phosphoric acid/steam heat exchanger, *Applied Thermal Engineering*, 2024, **248**, 123255, doi: 10.1016/j.applthermaleng.2024.123255.
[26] S. Barhatte, M. Lele, Investigations on microchannel heat exchanger using numerical, experimental, and ANN techniques, *Indian Journal of Engineering*, 2024, **21**, 1-15, doi: 10.54905/disssi.v21i55.e7ije1682.
[27] H. Al-Rawashdeh, Designing a virtual laboratory of the heat exchanger experiment by artificial neural network (ANN), *International Conference on Trends and Innovations in Management, Engineering, Sciences and Humanities*, London, June 24-27, 2024, doi: 10.37082/ijirmps.ictimesh-24.5.
[28] P. Naphon, T. Arisariyawong, Heat transfer analysis using artificial neural networks of the spirally fluted tubes, *Journal of Research and Applications in Mechanical Engineering*, 2016, **4**, 135-147, doi: 10.14456/jrame.2016.14.
[29] P. Naphon, S. Wiriyasart, T. Arisariyawong, L. Nakharintr, ANN, numerical and experimental analysis on the jet impingement nanofluids flow and heat transfer characteristics in the micro-channel heat sink, *International Journal of Heat and Mass Transfer*, 2019, **131**, 329-340, doi: 10.1016/j.ijheatmasstransfer.2018.11.073.
[30] P. Vengsungnle, N. Naphon, S. Poojeera, A. Srichat, P. Naphon, Artificial neural network, experimental and numerical study on air cooling rubber mattresses for elderly and bedridden patients, *Engineered Science*, 2024, **32**, 1301, doi: 10.30919/es1301.
[31] P.Vengsungnle, N.Naphon, S.Poojeera, J.Jongpluempiti, A.Srichat, S.Eiamsa-ard, P.Naphon, Heat transfer and flow analysis for square tube with oscillating electromagnetic field with experimental data by artificial neural network, *Cogent Engineering*, 2024, **11**, doi: 10.1080/23311916.2024.2430431.
[32] P. Naphon, S. Wiriyasart, T. Arisariyawong, Artificial neural network analysis the pulsating Nusselt number and friction factor of TiO_2/water nanofluids in the spirally coiled tube with magnetic field, *International Journal of Heat and Mass Transfer*, 2018, **118**, 1152-1159, doi: 10.1016/j.ijheatmasstransfer.2017.11.091.
[33] S. A. Kalogirou, Applications of artificial neural-networks for energy systems, *Applied Energy*, 2000, **67**, 17-35, doi: 10.1016/s0306-2619(00)00005-2.
[34] N. Bar, T. K. Bandyopadhyay, M. N. Biswas, S. K. Das, Prediction of pressure drop using artificial neural network for non-Newtonian liquid flow through piping components, *Journal of Petroleum Science and Engineering*, 2010, **71**, 187-194, doi: 10.1016/j.petrol.2010.02.001.

Publisher's Note: Engineered Science Publisher remains neutral with regard to jurisdictional claims in published maps and institutional affiliations.

Open Access
This article is licensed under a Creative Commons Attribution-NonCommercial-NoDerivatives 4.0 International, which permits the use, sharing, adaptation, distribution and reproduction in any medium or format, as long as appropriate credit to the original author(s) and the source is given by providing a link to the Creative Commons license. This usage for commercial purposes is not allowed. If modifications, adaptations or any other transformation were made, it is not allowed for distribution. The images or other third-party material in this article are included in the article's Creative Commons license, unless indicated otherwise in a credit line to the material. If material is not included in the article's Creative Commons license and your intended use is not permitted by statutory regulation or exceeds the permitted use, you will need to obtain permission directly from the copyright holder. To view a copy of this license, visit https://creativecommons.org/licenses/by-nc-nd/4.0/.

©The Author(s) 2025.